Fractal Surface Reconstruction with Uncertainty Estimation: Modeling Natural Terrain

Kenichi Arakawa and Eric Krotkov

October 1992
CMU-CS-92-194

School of Computer Science
Carnegie Mellon University
Pittsburgh, PA 15213

This research was partially supported by NASA under Grant NAGW-1175. The views and conclusions contained in this document are those of the authors and should not be interpreted as representing the official policies, either expressed or implied, of NASA or the U.S. government.

Keywords: Fractal, **regularization, surface reconstruction, uncertainty**

Abstract

This report develops a systematic method, based on fractal geometry, for modeling natural terrain. The method consists of two main parts: reconstructing dense surfaces from sparse data while preserving roughness, and estimating the uncertainty of each reconstructed point.

In earlier work, Szeliski developed stochastic regularization techniques to reconstruct natural surfaces. We found that these methods did not provide sufficient control over the roughness of the reconstructed surfaces. We present a modified version in which a temperature parameter, determined as a function of the fractal dimension, plays a critical role in controlling roughness.

Reconstructing dense, rough surfaces is seldom useful without assigning some measure of confidence to the surface points. This is particularly challenging for the reconstructed points. We revisit Szeliski's approach of Monte Carlo estimation of uncertainty, and report quantitative accuracy results for both synthetic data and real range data.

Contents

List of Figures

List of Tables

1 Introduction

The fractal geometry described by Mandelbrot [12, 13] has been widely applied to natural pattern modeling. In earlier work [1], we developed a method to estimate the fractal dimension of natural terrain from sensed depth data, and showed that the estimated fractal dimension correlated strongly with the roughness perceived by human observers. In this report, we employ the computed fractal dimension for estimating (i) surface geometry, and (ii) its uncertainty (Figure 1).

Knowledge, even quite primitive knowledge, of surface geometry enables a wide variety of tasks involving interaction with the environment. For example, a mobile robot requires such information to plan and execute collision-free trajectories.

In estimating surface geometry, we consider the problem of constructing dense elevation maps of natural surfaces, given sparse and irregularly spaced depth data. We call this the ***natural surface reconstruction problem***. This problem (stated in the next section) differs from the traditional surface reconstruction problem in requiring that the reconstructed surface realistically reflect the rough, original surface. In contrast to approaches to surface reconstruction that impose smoothness constraints, our approach to natural surface reconstruction imposes roughness constraints.

An effective estimate of the uncertainty on surface geometry is valuable for many tasks, including obstacle avoidance, calculating search regions, robustness, and performance improvement. For example, a walking robot that uses force sensors on its feet might have to reduce its leg speed in order to prevent excessive ground contact forces. With a representation of the ground surface that explicitly included uncertainty (say, derived from an imaging sensor), the robot could increase its velocity and advance more safely by moving the legs at maximum speed until its feet were close (say, within 3σ) to the ground, and then slowing down.

In estimating the uncertainty on the reconstructed surface height values, we consider the problem of propagating uncertainty values from measured data to reconstructed data. This problem differs from traditional uncertainty analysis, which uses sensor models to identify bounds or distributions on surface measurements. Here the issue is to estimate the uncertainty on reconstructed (not measured) surface height values. This requires accounting for processing errors introduced in surface reconstruction, as well as measurement errors.

This report is organized as follows. In the next section, it presents a surface reconstruction

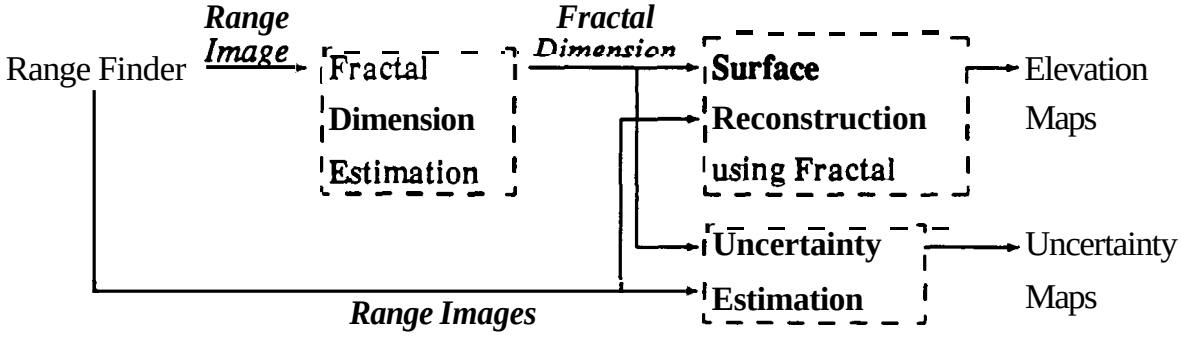

Figure 1: Approach to modeling natural terrain based on fractal geometry

technique that computes elevation maps at arbitrary resolution, yet preserves the roughness of the original pattern. In Section 3, it develops a method to estimate the uncertainty of both sensed and reconstructed elevation values, and evaluates the results qualitatively and quantitatively. In the final section, it summarizes the findings and identifies directions for future research.

2 Fractal Reconstruction of Natural Surfaces

Laser rangefinders and camera-based computer vision systems typically acquire depth data in a sensor-centered spherical coordinate system. As one would expect, regularly spaced samples in the spherical system map onto irregularly spaced samples in a Cartesian system. For example, Figure 2 illustrates how, in a Cartesian system, a sensor acquires denser range data from closer objects, and sparser range data from farther objects. This example shows that in order to build dense elevation maps, surface reconstruction is necessary.

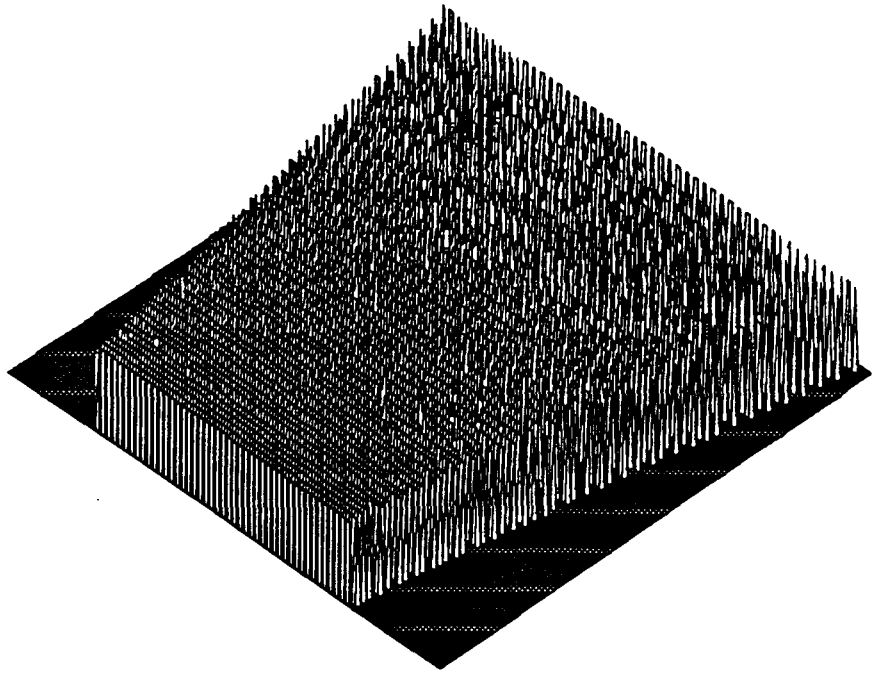

Figure 2: Typical sampling pattern for rangefinder or camera
This figure shows the elevations in a Cartesian system when a scanning rangefinder observes a horizontal plane. The sensor acquires denser range data from closer objects, and sparser range data from farther objects.

The surface reconstruction problem can be formulated as follows. Given a scattered set of surface elevation measurements, produce a complete surface representation satisfying three conditions:

- It must take the form of a dense array of inferred measurements with regular spacing.

- It must pass approximately through the original data points.
- It must be smooth where new points are inferred.

The surface reconstruction problem may be called a fitting problem by computer graphics researchers, and an approximation problem by others. It is closely related to the surface interpolation problem, for which the second condition requires the surface to pass exactly through the original data points.

The smoothness constraint in the third condition is inappropriate for natural surfaces, which as a rule exhibit roughness over a wide range of scales [6]. Thus, for the *natural* surface reconstruction problem, the third condition above becomes the following:

- It must be realistically rough where new points *are* inferred

This revised condition imposes a requirement that the roughness of the original pattern be known. In turn, this imposes a requirement that the surface reconstruction techniques adapt in a non-uniform manner to the roughness of the original pattern.

A powerful tool for modeling roughness is the degree of self-similarity, or fractal dimension. In earlier work [1], we developed a method to estimate the fractal dimension of range data from a laser rangefinder sensing rough terrain. In this paper, we use that estimated fractal dimension to control the roughness of the reconstructed surfaces. Specifically, we estimate the fractal dimension at a coarse scale (given by the spacing of the sensed range data) and use it at a finer scale (between range data samples). This approach relies on the property that as scale changes, the fractal dimension does not.

21 Related Work

The surface reconstruction problem has been formulated as an optimization problem, and solutions have been obtained through relaxation methods. For example, Grimson [9] suggested that given a set of scattered depth constraints, the surface that best fits the constraints passes through the known points exactly and minimizes the quadratic variation of the surface. He employed a gradient descent method to find such a surface. Extending this approach to use multi-resolution computation, Terzopoulos [21] proposed a method minimizing the discrete potential energy functional associated with the surface. In this formulation, known depth and/or orientation constraints contribute as spring potential energy terms. Poggio et al. [16] reformulated these approaches in the context of regularization.

Discontinuities in the visible surface have been a central concern in the approaches taken by Marroquin with Markov Random Fields [14], by Blake and Zisserman with weak continuity constraints [4], and by Terzopoulos with continuation methods [23].

Burt [7] developed a method that relies on locally fitting polynomial sufaces to the data. The method achieves computational efficiency through computation by parts, where the value computed at a given position is based on previously computed values at nearby positions.

Boult [5] developed surface reconstruction methods based on minimization with semi-reproducing kernel splines, and with quotient reproducing kernel splines. He compared the time and space complexity of these and other methods for a number of different cases.

Stevenson and Delp [18] presented a two-stage algorithm for reconstructing a surface from sparse constraints. The first stage forms a piecewise planar approximation to the surface, and the second stage performs regularization using a stabilizer based on invariant surface characteristics. By virtue of the selection of stabilizer, the algorithm is approximately invariant to rigid 3D motion of the surface.

The natural surface reconstruction problem has received less attention than the surface reconstruction problem. In the field of approximation, Barnsley [2] introduced iterated function systems with attractors that are graphs of a continuous function f that interpolate a given data set $\{(x_i, y_i)\}$ so that $f(x_i) = y_i$. It appears that these functions are well-suited for approximating fractal functions. Barnsley concentrated on existence proofs and moment theory for these functions, and there does not appear to be a firm connection to the issues at hand.

Yokoya et al. [24] present a technique for interpolating shapes described by a fractional Brownian function. The technique follows a random midpoint displacement approach [17]. At each level of recursion, the midpoint is determined as a Gaussian random variable whose expected value is the mean of its four nearest neighbors. Next, the technique displaces this midpoint by an amount that depends on the fractal dimension and the standard deviation of the fractional Brownian function. Thus, their technique is both stochastic and adaptive. However, there are two key limitations:

1. The technique requires an q u a l spacing between samples of the original pattern.

2. The technique cannot generate stationary random fractals. This is a result of a compromise between computational expense and generality.

Szeliski [20] showed that regularization based on the thin-plate model and weak-membrane model generates fractal surfaces whose fractal dimensions are 2 and 3, respectively. He then developed a probabilistic method for visual surface reconstruction using Maximum A Posteriori (MAP) estimation based on the fractal prior (see Section 2.2). The method generates surfaces whose fractal dimension lies between 2 and 3. Szeliski's approach provides the central inspiration for this paper. The contribution of our work is to extend his approach, amending a number of technical details concerning the temperature parameter, and applying the extended approach to non-synthetic range data from natural *terrain.*

2.2 Regularization using Fractal Priors

Szeliski [19, 20] developed a Bayesian framework for interpolating sparse elevation data that uses MAP estimation, and fractal prior distributions. In his formalization, the maximization of a posteriori probability is similar to the minimization of energy performed by regularization. For energy minimization, he employs a multigrid representation of the data called the *relative multiresolution decomposition.* For surface reconstruction, he minimizes the energy in each layer l (from the coarsest layer to the finest layer)

$$E^l(\mathbf{u}_l) = E_d(\mathbf{I}\mathbf{u}_l, \mathbf{d}) + E_p^l(\mathbf{u}_l)/T_p \,. \tag{1}$$

The term E_d in (1) is the data compatibility energy

$$E_d = \frac{r}{2} \sum_{(i,j)} c_{i,j}(u_{i,j} - d_{i,j}) ,$$

where $u_{i,j}$ is an absolute elevation computed using an interpolation matrix I that computes absolute elevations from the relative elevations in the multiresolution decomposition, and $d_{i,j}$ is a given elevation value. The term $c_{i,j}$ represents the confidence in $d_{i,j}$, typically given by the inverse of the measurement error.

The term $E_p(u)$ in (1) is the prior constraint energy, formulated as a blend of the thin-plate and weak-membrane models (called "splines under tension" by Terzopoulos [22])

$$E_p^l(u_l) = \frac{1}{2} \int \int [w_1^l(u_{lx}^2 + u_{ly}^2) + w_2^l(u_{lxx}^2 + 2u_{lxy}^2 + u_{lyy}^2)] dx\, dy ,$$

where the weights are

$$w_1^0 = |2\pi f_0| w_2^0 , \tag{2}$$

$$w_m^{l+1} = 2^{2(m+D-4)} w_m^l , \tag{3}$$

and D is the fractal dimension.

The parameter T_p in (1) is similar to the temperature for the Gibbs Sampler developed by Geman and Geman [8]. At higher temperatures, the local conditional probability distributions become more uniform.

Using (2), Szeliski found empirically that minimizing the energy of only the finest layer, the prior model behaves as a fractal whose dimension is D in the vicinity of frequency f_0. Equation (3) changes the frequency, thus varying the fractal dimension of different resolutions in the multiresolution decomposition.

Szeliski applied Gauss-Seidel relaxation for energy minimization. The energy can be rewritten in the quadratic form

$$E(u) = \frac{1}{2}\mathbf{u}^T\mathbf{A}\mathbf{u} - \mathbf{u}^T\mathbf{b} + c \tag{4}$$

$$= \frac{1}{2}(\mathbf{u} - \mathbf{u}^*)^T\mathbf{A}(\mathbf{u} - \mathbf{u}^*) + k , \tag{5}$$

with $\mathbf{A} = \mathrm{A}_p/T_p + \mathrm{A}_d$, $\mathbf{b} = \mathbf{A}_d\mathbf{d}$, and the optimal elevations that minimize the energy $\mathbf{u}^* = \mathbf{A}^{-1}\mathbf{b}$. Because the energy term is quadratic, the relaxation method reaches the minimum energy, and the optimal elevations are computed with $T_p = 0$.

The probability distribution corresponding to the energy function is

$$p(u_i|\mathbf{u}) \propto \exp\left(-\frac{a_{ii}(u_i - u_i^+)^2}{2T_p}\right) ,$$

which is a Gaussian with mean u^+ and variance T_p/a_{ii} (also called a Gibbs or Boltzmann distribution). Thus, setting T_p to a non-zero value changes the variance ("noise") of the reconstructed surface.

2.3 Effect of Temperature on Surface Reconstruction

The temperature parameter T_p controls the diffusion of the local energy distribution [20]. Do the fractal characteristics of the reconstructed surface depend on T_p?

To answer this question, we synthesized eight elevation maps with fractal dimensions varying from 2.1 to 2.8. We subsampled these elevation maps, set T_p to zero, and then reconstructed the subsamples. Figures 3–5 depict the reconstructed surfaces for fractal dimensions 2.3, 2.5, and 2.7. In each case, the reconstructed result is too smooth, as compared to the original synthetic patterns.

Figure 6 plots estimates of the fractal dimension of the eight reconstructed surfaces. The estimates of fractal dimension are computed here, and throughout this paper, by Yokoya's method [1,24]. More precisely, the figure illustrates the scaling characteristics of the underlying data: the abscissa represents logarithmic scale (e.g., over what size neighborhood is the estimate computed), and the ordinate represents logarithmic spatial variation (e.g., the amount of variation in surface elevation). If the underlying data possesses fractal characteristics, then the curve in the log-lot plot will be linear over a wide range of scales, and the slope of the line will vary inversely with the fractal dimension (the greater the slope, the smaller the fractal dimension).

Results for the eight original synthetic data sets appear on the left-hand side of Figure 6. The curves exhibit linear behavior over most scales; the departure from linearity at larger scales is an artifact of the technique for estimating the fractal dimension.

Results for the reconstructions appear on the right-hand side of Figure 6. To zeroth order, the curves are parallel, implying (incorrectly) that the surfaces have the same fractal dimension. To first order, analysis reveals that the slope in each of the plots is too steep at higher frequencies (smaller scales), i.e., the fractal dimension of the reconstructed surfaces is too low. This is also apparent, qualitatively, in the reconstructions shown in Figures 3–5. These results demonstrate that surface reconstruction using a temperature of zero produces overly smooth surfaces, at least at higher frequencies. Thus, the answer is affirmative to the question of the dependence of fractal characteristics on T_p.

Since setting T_p to zero produces unsatisfactory reconstructions, what is the proper T_p for a given fractal dimension D? To answer this question empirically, let $Syn()$ synthesize a dense fractal pattern of fractal dimension D, $Sub()$ subsample a pattern, $Rec()$ reconstruct a pattern using regularization with temperature T_p, and $Est()$ estimate the fractal dimension of a pattern (again, using Yokoya's method). Let $\hat{D}$ be given by

$$Est(Rec(Sub(Syn(D)),T_p)) = \hat{D} \ . \tag{6}$$

The proper temperature T_p for D is that which minimizes the difference between D and $\hat{D}$. When searching for the minimum difference, we use the estimated fractal dimension $D^* = Est(Syn(D))$ instead of D, because the estimated fractal dimension is apt to be smaller than the real fractal dimension, especially for $D > 2.5$.

Table 1 records seven empirically determined temperatures, and the differences between the fractal dimension of the original patterns and of the reconstructed results. All the differences are small, lending credence to the conclusion that setting T_p appropriately permits the method to preserve the roughness of the original patterns, even on reconstructed surfaces.

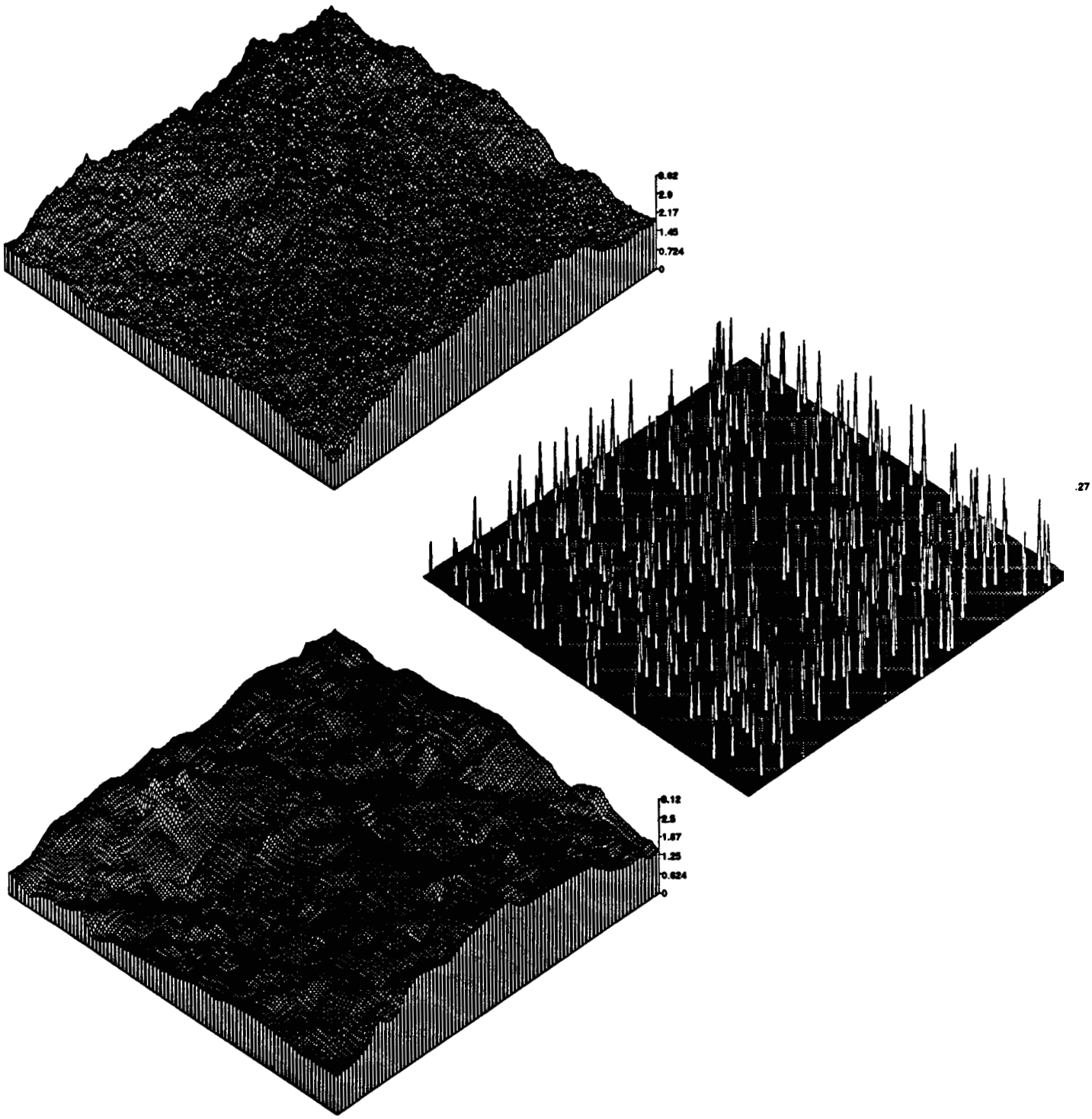

Figure 3: Reconstruction of synthetic surface (D=2.3) using Szeliski's method
Top *to* bottom: synthetic original, subsampled, and reconstructed surfaces.

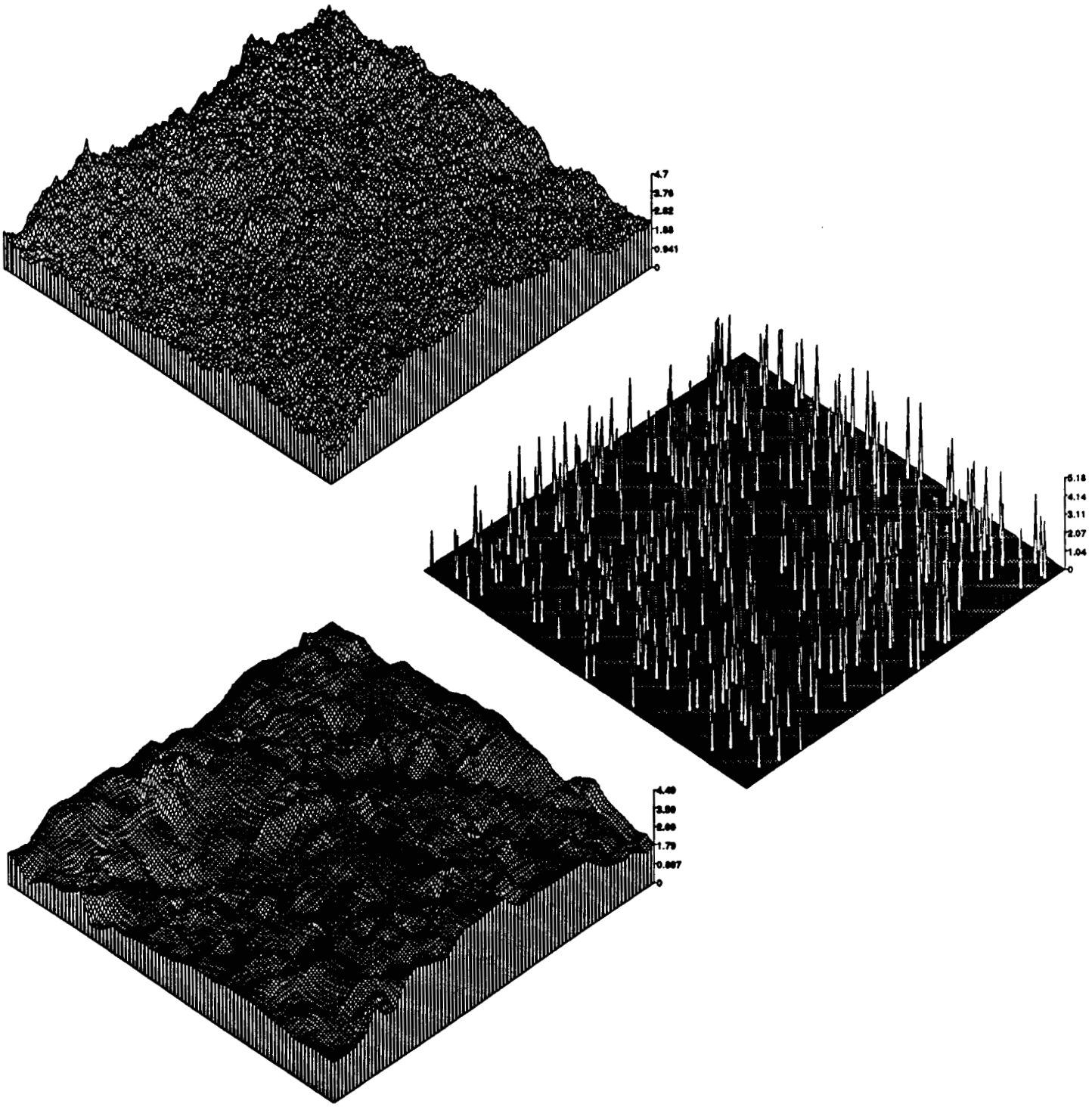

Figure 4: Reconstruction of synthetic surface (D=2.5) using Szeliski's method
Top to bottom: synthetic original, subsampled, and reconstructed surfaces.

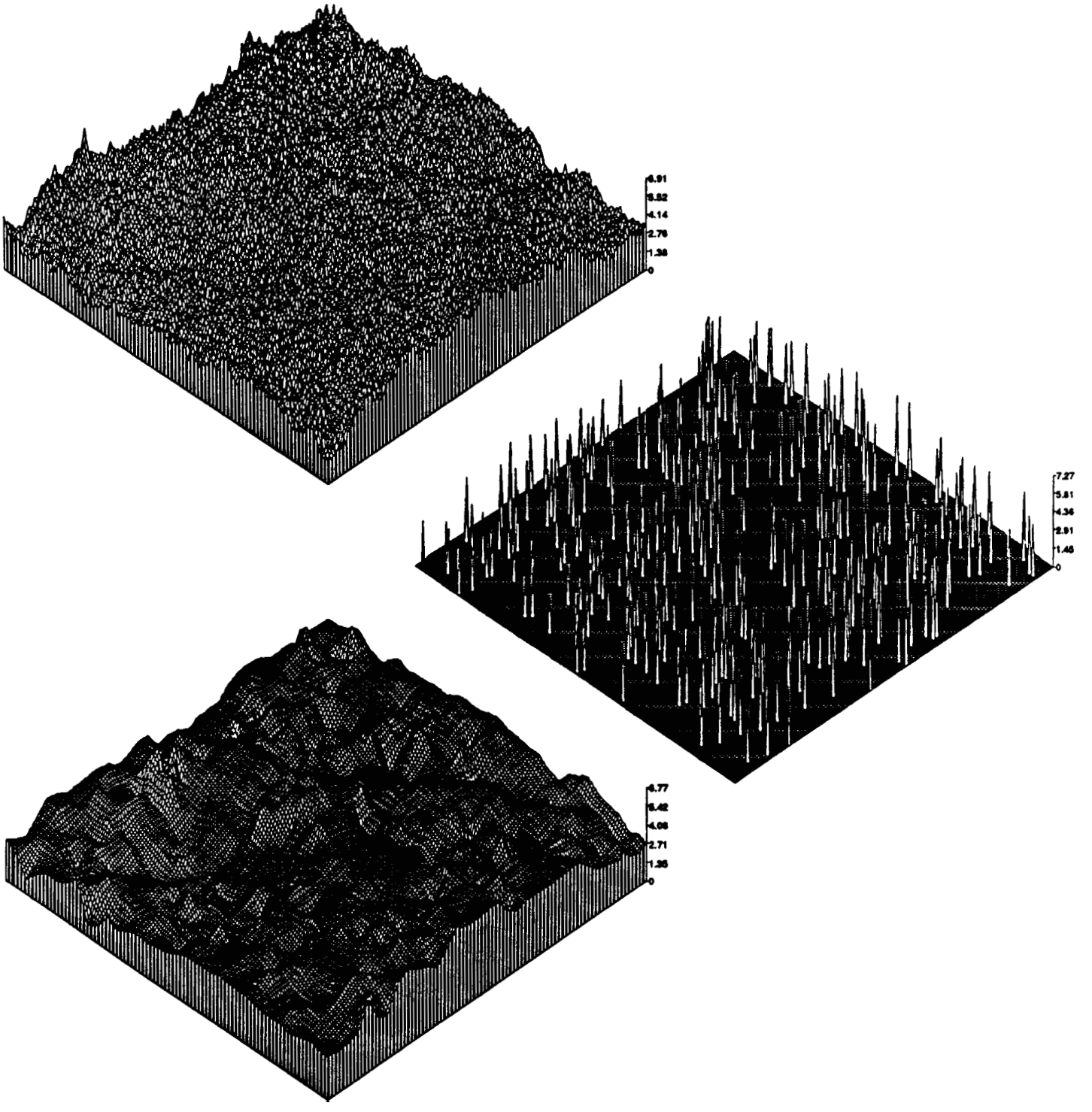

Figure 5: Reconstruction of synthetic surface (D=2.7) using Szeliski's method
Top to bottom: synthetic original, subsampled, and reconstructed surfaces.

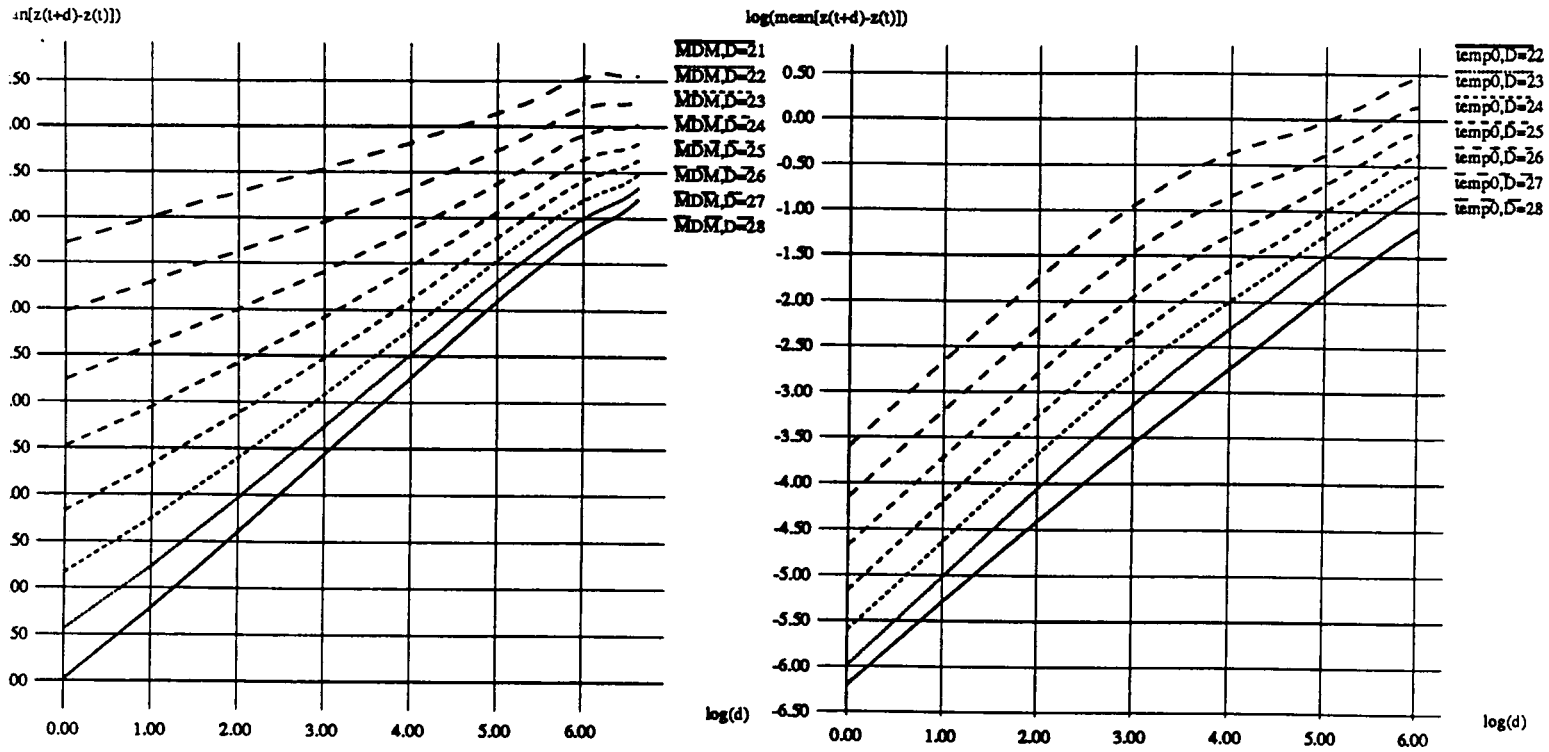

Figure 6: Scaling behavior of original (left) and reconstructed surfaces

Figure 7 shows surface reconstructions using three of the empirically determined temperatures. The reconstructed surfaces are reasonably rough compared to the original synthetic patterns.

Figure 8 plots the estimated fractal dimension of the reconstructed results. The curves display fairly linear behavior over most scales, and unlike the right-hand si& of Figure 6, they no longer appear parallel or exhibit steep slopes at higher frequencies.

D	T_p	$\lvert D - \hat{D} \rvert$
2.2	9.5×10^{-6}	7.0×10^{-3}
2.3	3.0×10^{-5}	2.1×10^{-2}
2.4	8.9×10^{-5}	3.0×10^{-3}
2.5	3.0×10^{-4}	1.9×10^{-2}
2.6	7.5×10^{-4}	8.0×10^{-3}
2.7	3.0×10^{-3}	1.0×10^{-3}
2.8	9.5×10^{-3}	5.1×10^{-2}

Table 1: Temperatures determined empirically for synthetic data

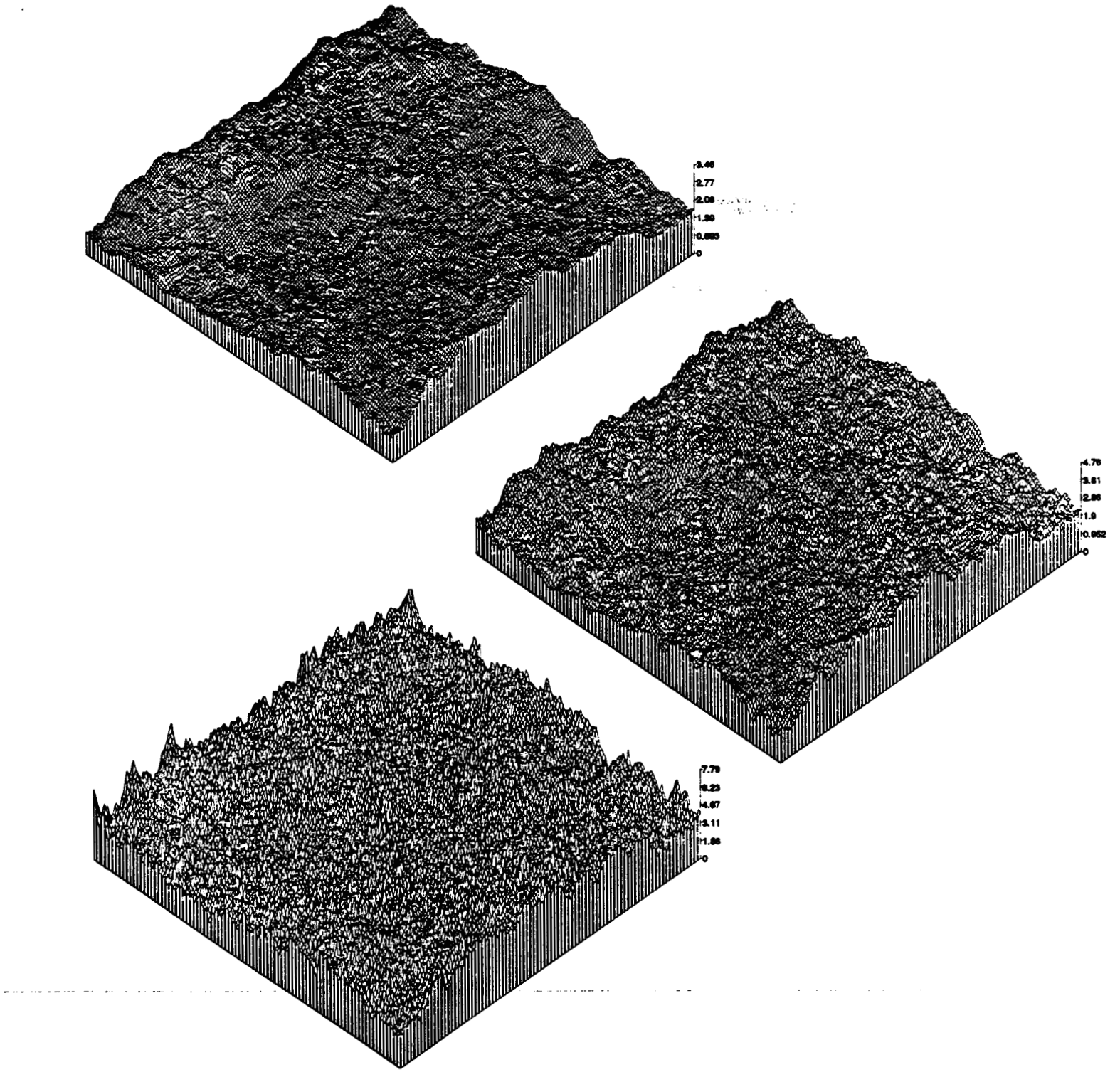

Figure 7: Surfaces reconstructed **from synthetic** data **using non-zero temperatures**
From top to bottom, **the** fractal **dimensions are set to 2.3, 2.5 and 2.7. The original synthesized and subsampled elevations are the *same* as for** Figures **3–5.**

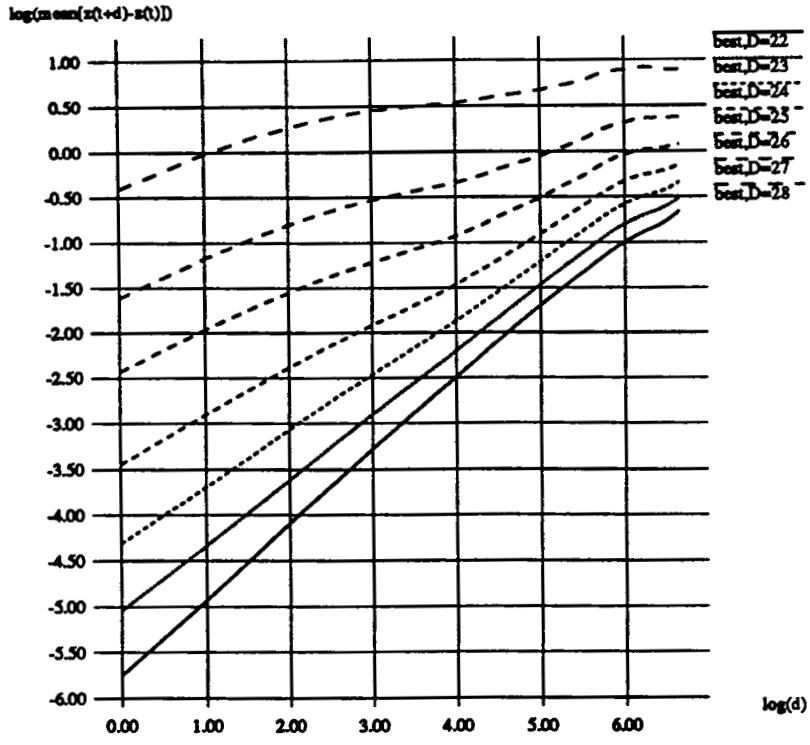

Figure 8: Scaling behavior of reconstructions using non-zero temperatures

2.4 Temperature as a Function of Fractal Dimension

The results from the previous section demonstrate control over the fractal characteristics of the reconstructed surface by setting appropriate non-zero temperatures. However, the temperatures do not appear to have any meaning regarding fractal dimension; the temperatures simply control the amount of local diffusion [20]. In this section, we formalize the temperatures as a function of fractal dimension using an analogy to the Successive Random Addition (SRA) method of synthesizing fractal patterns [17].

The SRA method synthesizes fractional Brownian motion. It adds normally distributed random values to elevations in the multigrid representation. The variances are controlled according to the resolution of each layer l by

$$\sigma^2 = \frac{\sigma_0^2(1 - 2^{4-2D})}{2^{(6-2D)l}},$$

where D is the fractal dimension of the pattern to be synthesized.

Szeliski's method adds a normally distributed random value to the elevations of each layer in the multigrid representation by setting a non-zero temperature T_p. The temperature is proportional to the variance of the Gaussian, and controls the amount of diffusion in the high-frequency domain. His method uses the same temperature (same variance) for all layers.

In order to synthesize patterns that preserve fractalness at higher frequencies, we set the temperature T_{pl} at each layer l by analogy with the SRA method:

$$T_{p0}(D) = k\sigma_0^2(1 - 2^{4-2D}), \quad (7)$$

D	D^*	T_{p0}	$\lvert D^* - \hat{D} \rvert$
2.2	2.236	4.4×10^{-6}	6.0×10^{-2}
2.3	2.308	1.5×10^{-5}	4.4×10^{-2}
2.4	2.390	4.5×10^{-5}	2.6×10^{-2}
2.5	2.476	1.4×10^{-4}	1.8×10^{-2}
2.6	2.561	4.1×10^{-4}	1.7×10^{-2}
2.7	2.643	1.3×10^{-3}	3.5×10^{-2}
2.8	2.716	3.8×10^{-3}	5.6×10^{-2}

Table 2: Temperatures determined by new formalization for synthetic data

$$T_{pl}(D) = T_{pl-1}(D)2^{6-2D}, \tag{8}$$

where $T_{p0}(D)$ is the temperature for the finest-resolution layer, and σ_0 is the standard deviation of elevation values sampled at the finest resolution.

The two unknowns are σ_0 and k. Pentland's method for fractal dimension estimation [15] directly computes the parameter σ_0. To compute k, it suffices to know one temperature $T_{p0}(D)$, and then to follow the iterative method taken in the previous section to determine the proper temperatures.

To test this formalization of temperature as a function of fractal dimension, we applied it to three different types of data: synthetic data, range data from a scanning laser rangefinder, and digital terrain map data.

For synthetic data, we first determined $T_{p0}(D)$ for D = 2.4. From this known temperature, it follows that $k = 4.7 \times 10^{-7}$. Using this value of k, Equations (7) and (8) compute temperatures for different D. Table 2 records the computed temperatures, as well as the difference between the fractal dimension $D^* = Est(Syn(D))$ and the fractal dimension $\hat{D}$ given by (6). The differences between D^* and $\hat{D}$ are negligible.

Figure 9 illustrates the surfaces reconstructed using these new temperatures. The surfaces appear appropriately rough and highly realistic. Figure 10 plots the estimated fractal dimension of the reconstructed surfaces. It shows that the reconstructed surfaces maintain linearity over a wide range of scales.

We acquired range data from laser rangefinder images of a test area with sand on the ground, and some meter-scale rocks. We selected a relatively smooth area of the terrain consisting mainly of sand. We computed the proper temperature for this pattern and calculated[1] k as 4.0×10^{-2}. Table 3 shows the temperatures computed using this value of k. The differences between D^* and $\hat{D}$ are comparable to those observed for synthetic data (Table 2).

Figure 11 shows three reconstructed surfaces. The top surface is reconstructed from data corresponding to a rougher area of the terrain consisting mainly of rocks, and the other surfaces are reconstructed from data corresponding to smoother areas consisting mainly of sand. Using the same

[1] The parameter A is constant for patterns of any fractal dimension, so long as they are generated by the same process. For this new data, a different generating process acts. Therefore, we must recompute A.

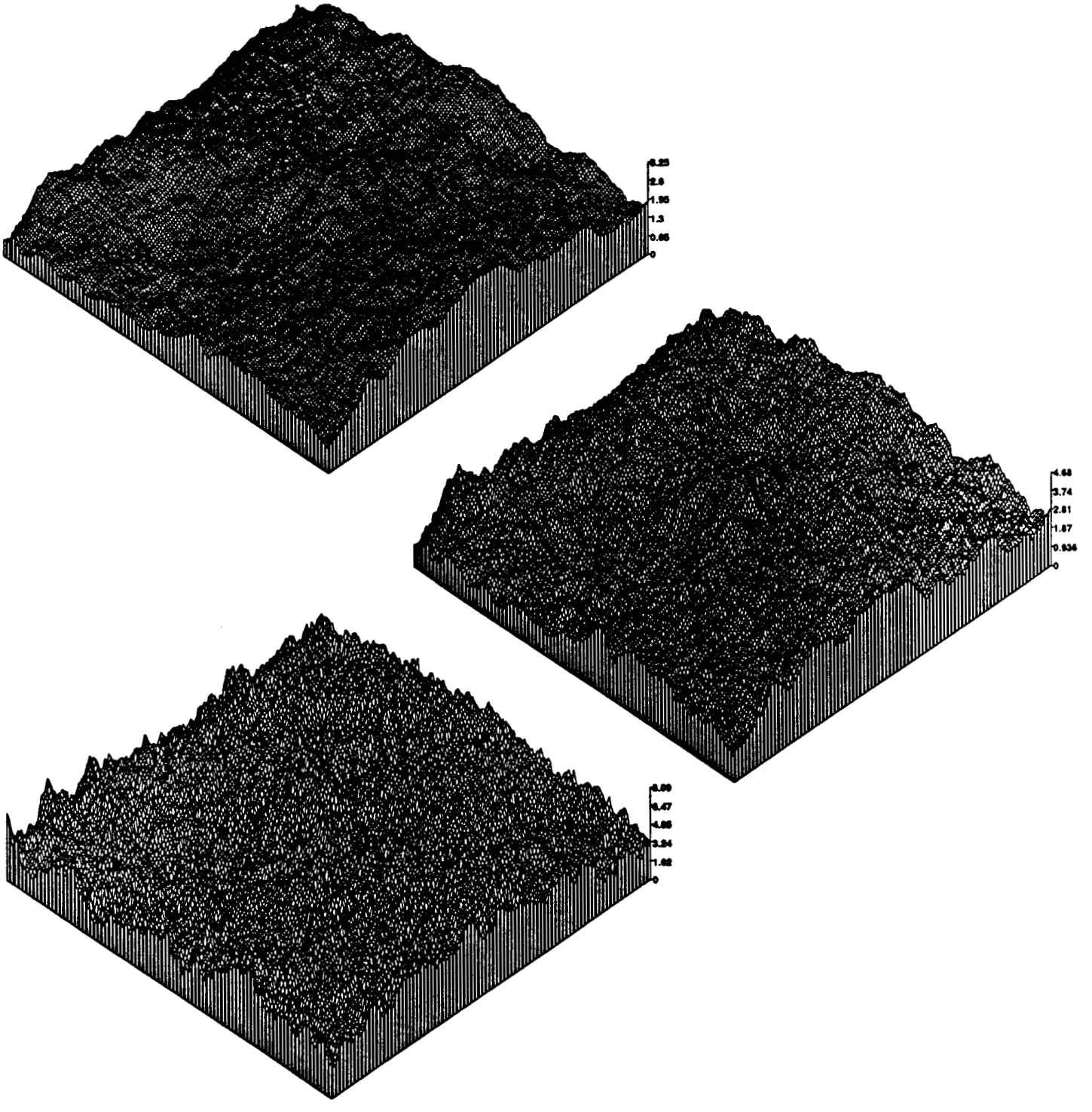

Figure 9: Surfaces reconstructed using temperatures computed by new formalization From top to bottom, the *fractal* dimensions are set to 2.3, 2.5 and 2.7. The original synthesized and subsampled elevations are the same as for Figures 3–5.

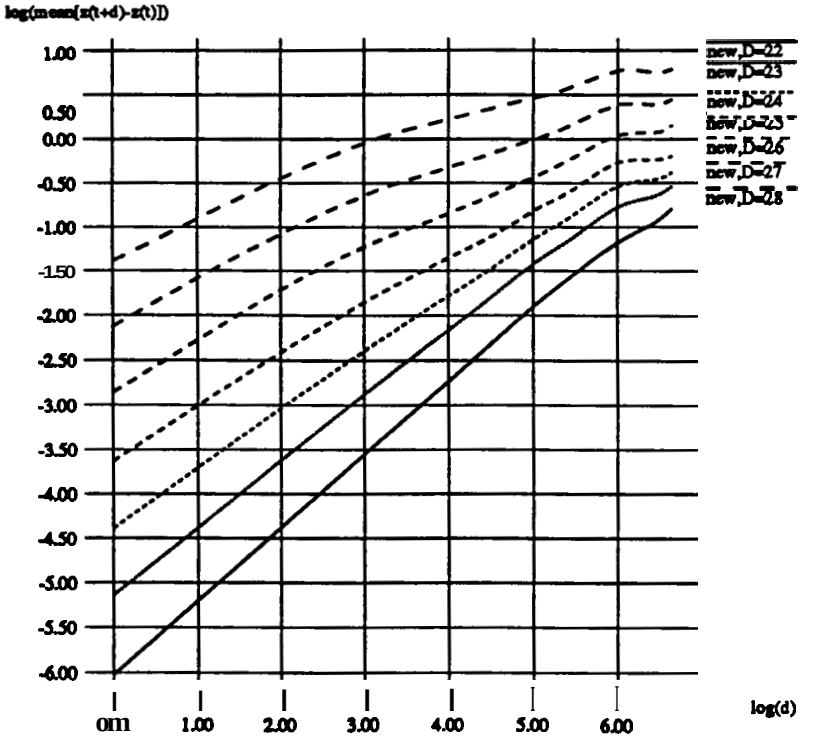

Figure 10: Scaling behavior of surfaces reconstructed using new temperatures

D^*	T_{p0}	$\lvert D^* - \hat{D}\rvert$
2.12	1.0×10^{-7}	1.0×10^{-1}
2.23	1.8×10^{-7}	4.5×10^{-2}
2.51	1.0×10^{-4}	1.6×10^{-2}

Table 3: Temperatures determined by new formalization for range data

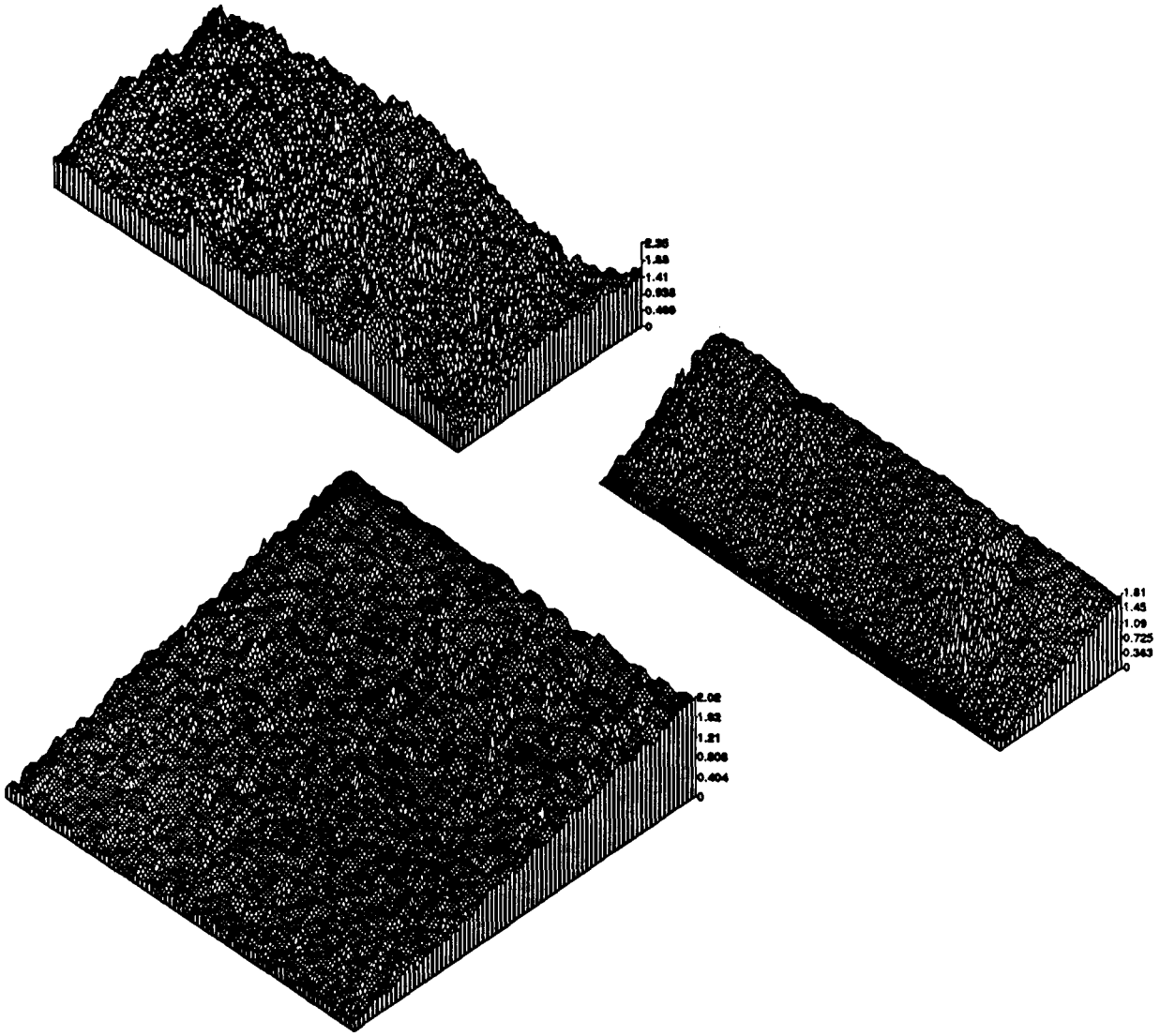

Figure 11: **Surfaces** reconstructed from range data
The range data was acquired for rocky terrain (top) and two different sandy terrains.

parameters (k, σ_0, T_{p0}), the method adapts **to** the roughness of the **original** surface, reconstructing the rocky area rather roughly, **and** reconstructing the **sandy** area rather smoothly.

Figure **12** plots the scaling behavior of the reconstructed elevation maps. These are not **as** linear **as** for the synthetic **data.** However, they **do** exhibit enough of **a** linear tendency to demonstrate scale-invariance.

We **acquired digital** terrain data **from an** aerial cartography database of Mount **Erebus, an** active volcano in **Antarctica. We** estimated the **fractal** dimension D^* **to** be approximately 2.3, with $\sigma_0 \approx 68.0$. We **used** the value of k determined above for **the** range data, **and** reconstructed the sparse **data.** Figure **13 shows** *that* the method produces **results that** *are* **dense and** fairly realistic, including even the shape of craters.

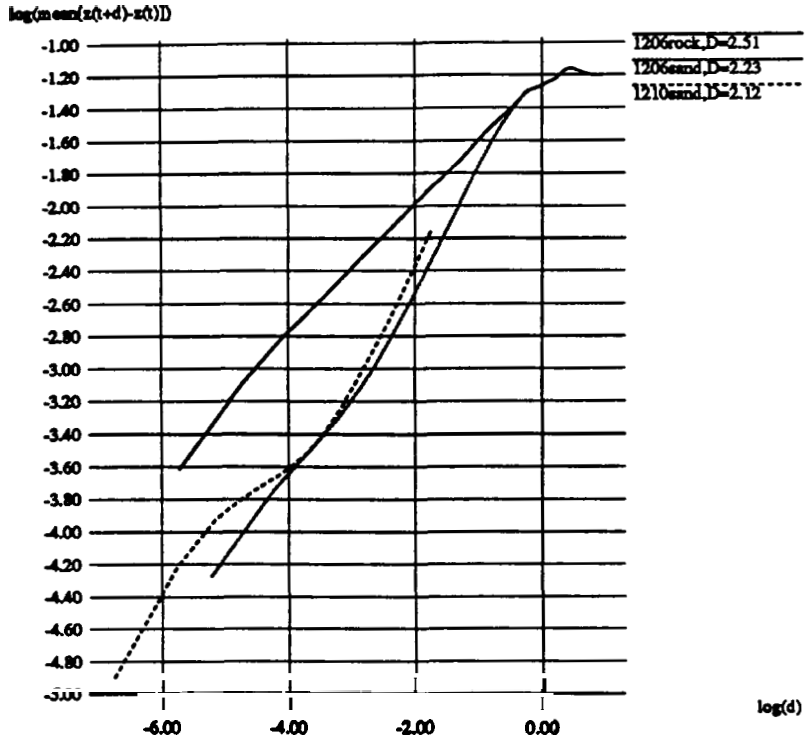

Figure 12: Scaling behavior of reconstructions from range data with new temperatures

3 Uncertainty Estimation

Suppose that we have a sensor that directly measures elevations, i.e., that produces as output an elevation map rather than a range image. With such a sensor, it is easy to determine the uncertainty of each elevation: this is just the measurement uncertainty predicted by a suitable sensor model [113. No processing error needs to be taken into account. However, with a sensor that produces as output a range image, it is more difficult to determine the uncertainty of each elevation, because two factors contribute to the uncertainty: sensor measurement noise, and processing error caused by surface reconstruction and coordinate transformations.

Szeliski addressed uncertainty estimation as a central issue (reviewed below). Like him, we estimate uncertainty using the same stochastic model used in the previous section for surface reconstruction. Our contribution is to carry Szeliski's work further, determining quantitatively the accuracy of the estimated uncertainty values, and applying the approach to non-synthetic data of natural terrain.

3.1 Related Work

Error propagation [3] is one obvious approach to the problem of estimating the uncertainty of reconstructed values. Suppose that a derived quantity x is a function of measured variables $x = f(u, v, \ldots)$. The error propagation technique identifies the uncertainty on x by approximating

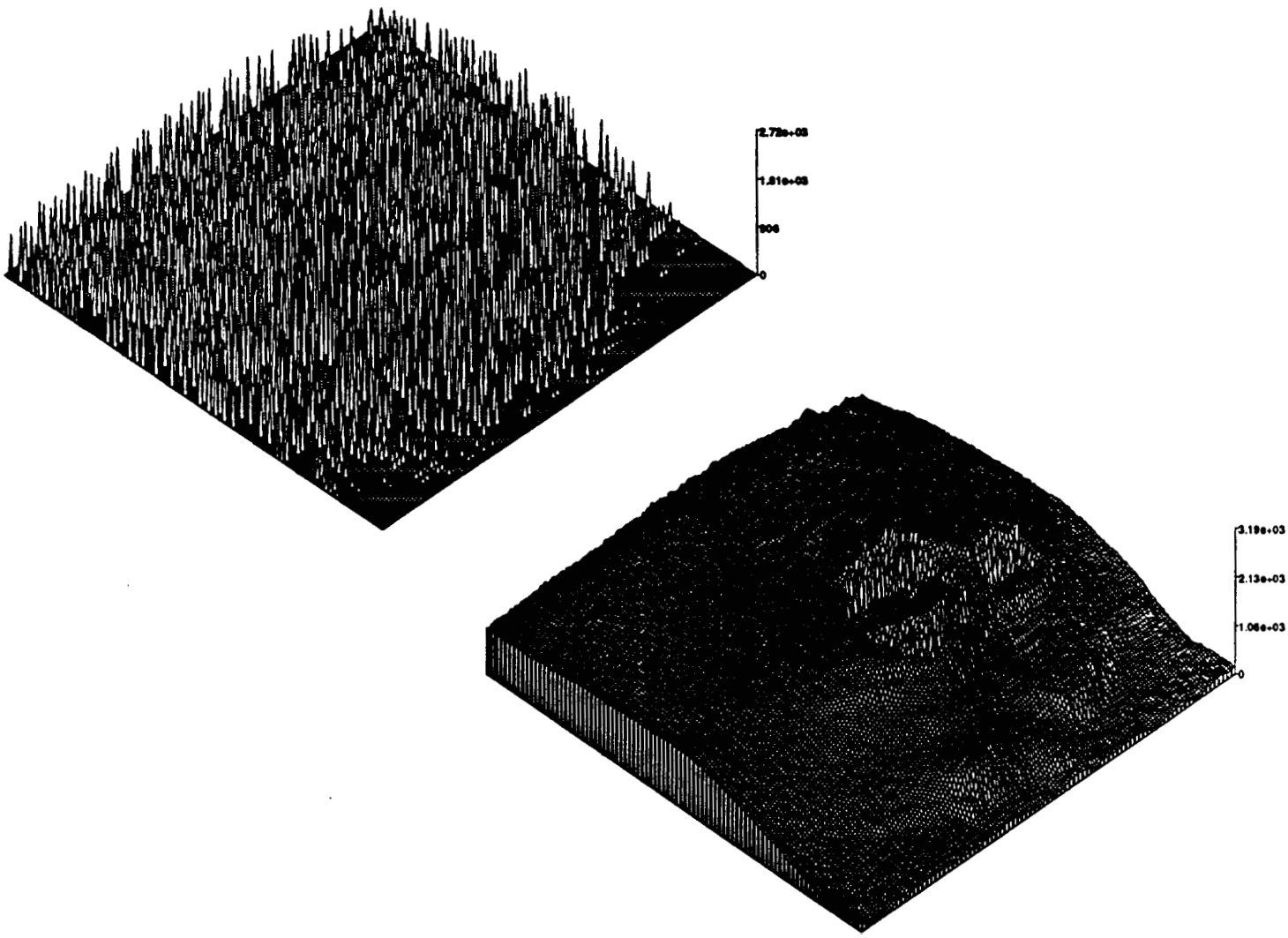

Figure 13: Surface reconstructed from digital terrain data for Mt. Erebus
Original elevation data (top) and reconstructed surface when the fractal dimension is set to 2.65.

the standard deviation σ_z

$$\sigma_z \approx \sigma_u^2(\frac{\partial Y}{\partial u})^2 + \sigma_v^2(\frac{\partial x}{\partial v})^2 + 2\sigma_{uv}^2(\frac{\partial x}{\partial u})(\frac{\partial Y}{\partial v}) + h.o.t.$$

Effectively, this propagates errors on the measured variables into the derived quantity. This technique does not account for uncertainty due to errors committed in the processing steps (as distinct from the sensing and measuring steps). For instance, it is insensitive to the interpolation rule, computing similar uncertainties for linear, quadratic, and other cases.

Keren and Werman [10] developed a technique for uncertainty estimation based on a variation on regularization. Their method addresses only the thin-plate model, and thus has limited applicability to the case of fractal models.

Szeliski [20] developed two techniques for estimating the uncertainty of reconstructed elevations: a deterministic approach that inverts a matrix, and an indirect computation of statistics using Monte Carlo estimation.

The deterministic approach estimates uncertainties by computing square roots of the diagonal elements of the matrix[2] A^{-1}. However, when the dimension of the finest-resolution elevation map is $n \times n$, then the dimension of A is n^4. Direct computation of the inverse matrix causes a computational explosion. For example, with a 512 x 512 elevation map, the number of entries in A is more than 10^{10}.

3.2 Monte Carlo Estimation of Uncertainty

An alternative to the deterministic approach is to perform surface reconstruction at non-zero temperatures as in the previous section (running the Multigrid Gibbs Sampler), and to estimate the desired statistics using a Monte Carlo approach. More precisely, during the energy minimization process at non-zero temperatures, we accumulate a running total of updated elevations and their squares. After a sufficient number of iterations, we compute the standard deviation of each elevation value from these totals.

To illustrate the Monte Carlo estimation approach, we synthesized a fractal terrain and subsampled it at regular intervals. Then we reconstructed the original surface using the sparse samples as input, and computed the uncertainty of each point on the reconstructed surface. Figure 14 illustrates the resulting uncertainty map, which exhibits a regular pattern, increasing away from known data points. Figure 15 examines this phenomenon in greater detail. For a single 255 element row, it plots the subsampled data points, the reconstructed elevation values, and the estimated uncertainties. The curve representing the reconstructed elevations passes through each of the data points, as required. The uncertainty increases with distance from the data points, as expected.

As another illustration, Figure 16 shows the results of applying the technique to real range data acquired by laser scanner images of a relatively smooth, sandy area. The figure shows the sparse elevations derived from the range images, the reconstructed surface and the estimated uncertainty.

[2] Recall that A is the sum of a matrix A_s of continuity stabilizers determined by the weights w_i in (2) and (3), and a matrix A_d of data confidence values. A^{-1} is the covariance of the multivariate Gaussian representing the a posteriori probability distribution corresponding to the energy $E(u)$ in (5).

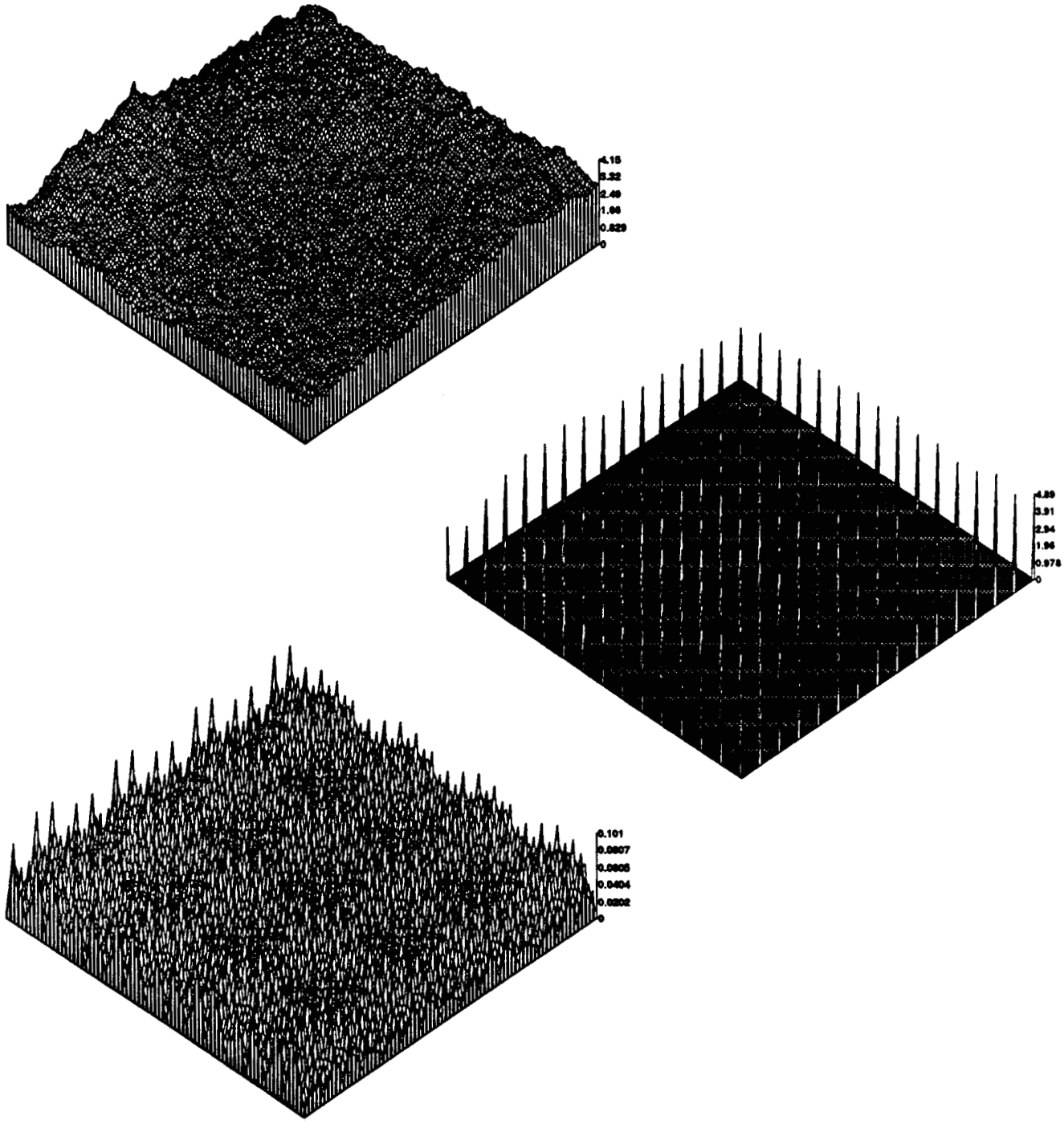

Figure 14: Uncertainty of elevations reconstructed from synthetic data (D=2.5) Synthesized fractal terrain (top), elevations subsampled regularly from 10x10 square region (middle), and resulting uncertainty map.

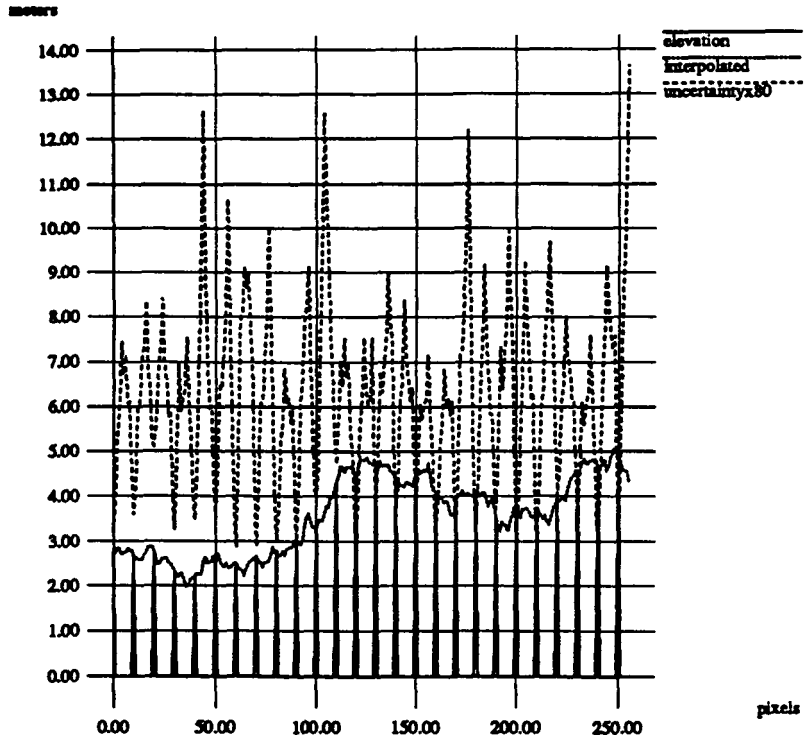

Figure 15: Sparse elevations, reconstructed values, and uncertainty along row 130

Again, it is clear from the uncertainty map that the uncertainty of a reconstructed elevation is higher when farther from sensed elevations, as expected, and as observed above in the case of synthetic data.

3.3 Quantitative Results

The two preceding illustrations indicate qualitatively the accuracy of the estimated uncertainty values. In order to assess the accuracy quantitatively, we synthesized an elevation map with fractal dimension 2.5. Then we subsampled the synthesized map, and reconstructed the sparse samples (like the experiment for Figure 14). Figure 17 plots the estimated uncertainty along the horizontal axis versus the difference (error) between the original and reconstructed elevations along the vertical axis. Further, the figure plots two linear functions $f_{min}(v) = -av$ and $f_{max}(v) = av$, where v is the uncertainty, a is 0.8. Almost all of the plotted points lie in the region defined by the linear functions, and their density decreases with their distance from the horizontal axis.

From the plots, we expected the distribution of the error to follow a Gaussian distribution $N(0, \sigma^2)$ with σ proportional to the uncertainty, namely

$$u_i - \hat{u}_i \sim N(0, (kv_i)^2) \ , \tag{9}$$

where u_i, $\hat{u}_i$, and v_i are the reconstructed elevation, the true elevation, and the estimated uncertainty of each position i.

We verified this expectation by performing a chi-square test on synthetic data generated with fractal dimension 2.5. Figure 18 illustrates the probability density function of $(u_i - \hat{u}_i)/v_i$ from

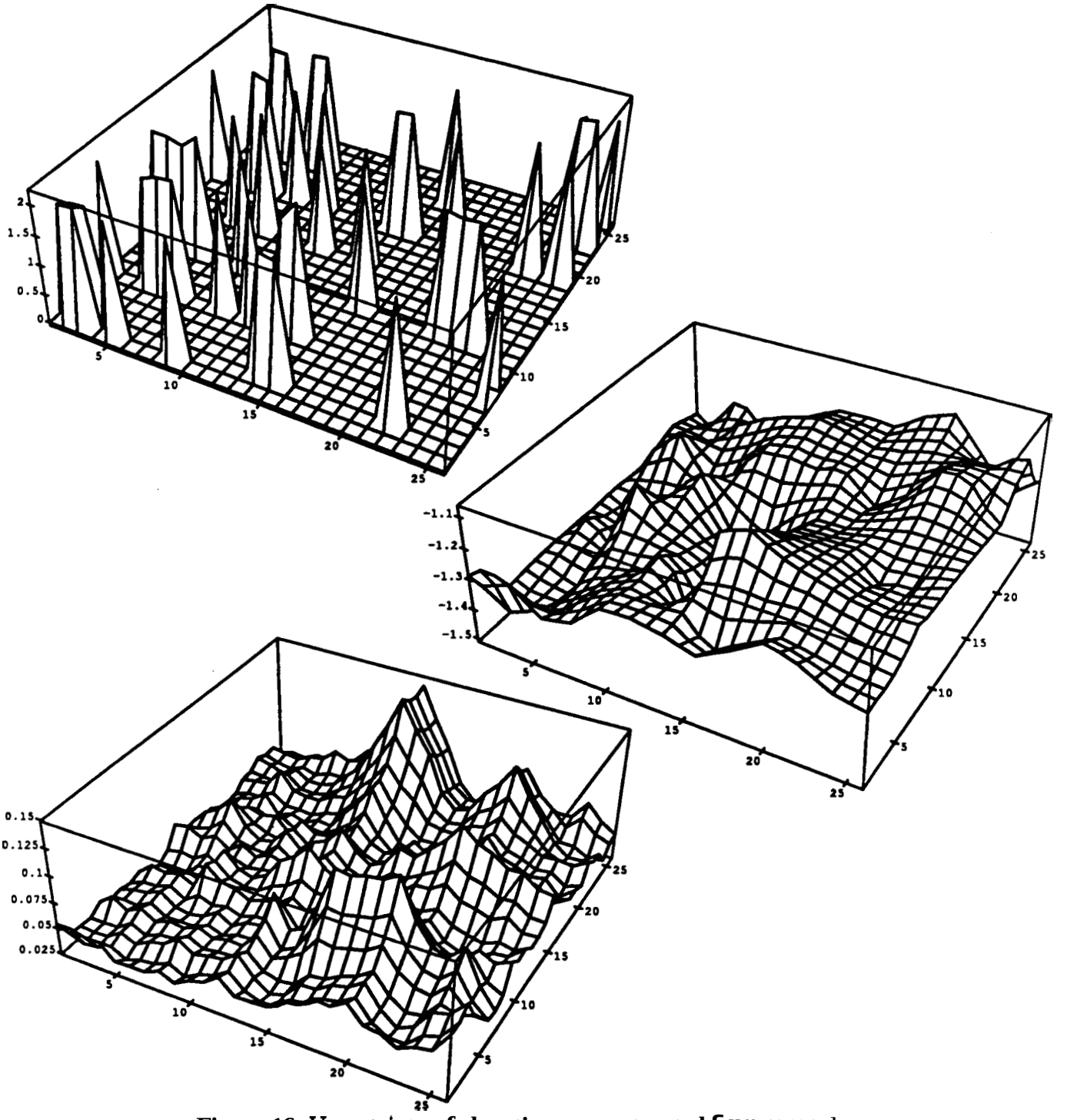

Figure 16: Uncertainty of elevations reconstructed from range data
Elevations derived from laser scanner range data (top), reconstructed elevations (middle), and resulting uncertainty **map.**

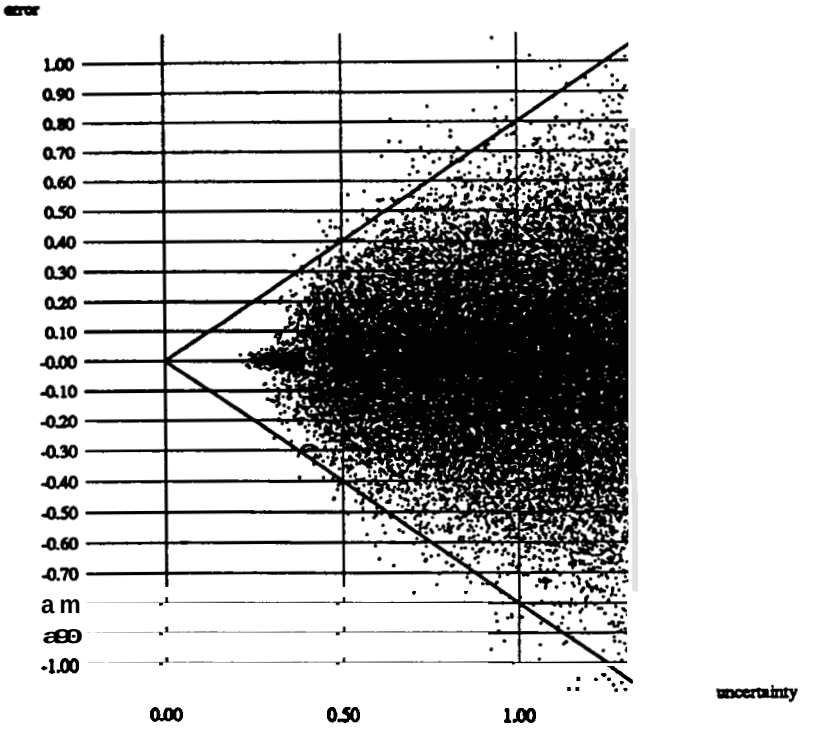

Figure 17: Estimated uncertainty versus true error

the sample, and shows as a dotted line the probability density function $N(-0.009, 0.263^2)$. We can regard the the mean as zero because its absolute value is very small compared to the standard deviation. The chi-square test rejects (at the 5% significance level) the null hypothesis that $(u_i - \hat{u}_i)/v_i$ does not obey the Gaussian distribution $N(0, 0.263^2)$. Note that the uncertainty v_i is regarded as a constant on each position i. Therefore, this suggests that the elevation error incurred by the surface reconstruction is distributed normally, with standard deviation proportional to the estimated uncertainty as (9) shows.

4 Discussion

In this report, we described an approach to modeling natural terrain using fractal geometry, which includes fractal surface reconstruction and uncertainty estimation. The main contributions are as follows:

- To reconstruct surfaces adaptively to the roughness of original sparse elevation data.
- To estimate dense uncertainty even on reconstructed elevations.

Surface reconstruction problems are ill-posed. They can be solved with strong enough constraints on the underlying surface being reconstructed. This report considers surfaces such as rugged, natural terrain, and adopts roughness constraints to be satisfied by The method produces

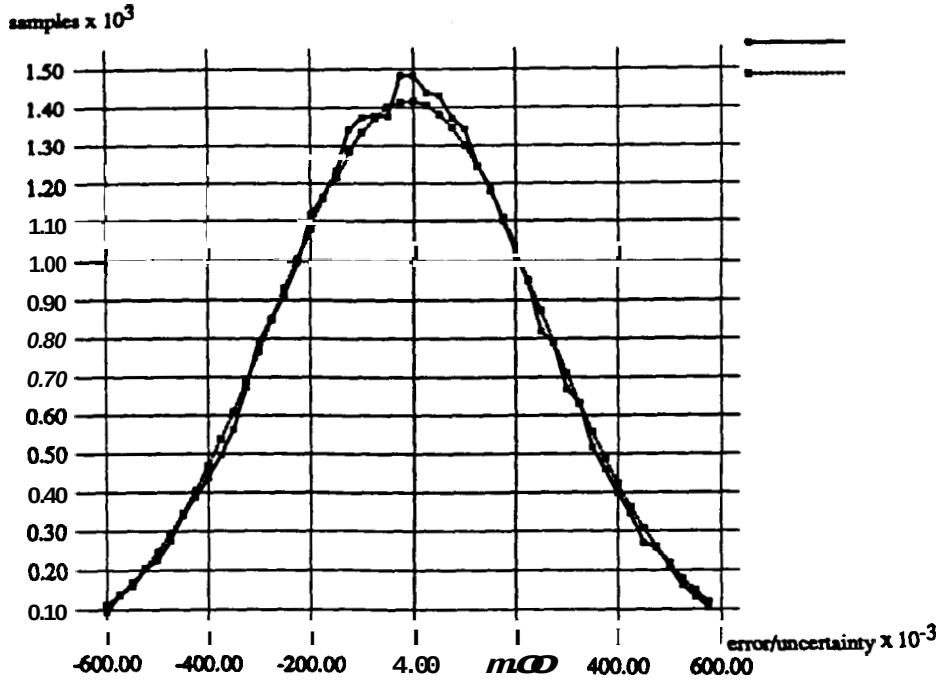

Figure 18: Probability density function of errors on reconstructed elevations
The number of samples is 37372. The dotted curve illustrates the pdf $N(-0.009, 0.263^2)$.

dense elevation maps with stochastic surface reconstruction. The reconstructed elevations are realistic, but not real.

As future work, we consider three topics. First, our surface reconstruction and uncertainty estimation approaches do not take discontinuities into account. Natural terrain contains many discontinuities, such as step edges around stones. Our method does not produce realistic results reconstructing sparse depth data with discontinuities. Many researchers have considered this problem, and have derived methods that we expect will fit well with our approach.

In nature, many patterns are not truly self-similar, but are anisotropic and/or multifractal.[3] Our approach cannot be applied to such patterns. In future work, we would like to remedy this situation.

Our approach requires large amounts of computation. Reconstruction of a 256 x 256 elevation map typically consumes around two hours on a Sun4/75 with 24MB physical memory. Uncertainty estimation consumes even more cycles. The basic ideas behind the surface reconstruction and the uncertainty estimation approaches can be implemented on massively parallel machines, reducing substantially the computation time.

[3] A fractal pattern whose fractal dimension changes with scale or changes spatially is called a multifractal.

References

[1] K. Arakawa and E. Krotkov. Estimating Fractal Dimension from Range Images of Natural Terrain. Technical Report CMU-CS-91-156, School of Computer Science, Carnegie Mellon University, Pittsburgh, July 1991.

[2] M. Barnsley. Fractal Interpolation Functions. *Constr. Approx.*, 2:303–329, 1986.

[3] P. Bevington. *Data Reduction and Error Analysis for the Physical Sciences.* McGraw-Hill, New York, 1969.

[4] A. Blake and A. Zisserman. *Visual Reconstruction.* MIT Press, Cambridge, Massachusetts, 1987.

[5] T. Boult. *Information-Based Complexity in Non-Linear Equations and Computer Vision.* PhD thesis, Department of Computer Science, Columbia University, 1986.

[6] P. Burrough. Fractal Dimensions of Landscapes and Other Environmental Data. *Nature,* 294:240–242, 1981.

[7] P. Burt. Moment Images, Polynomial Fit Filters, and the Problem of Surface Interpolation. In *Proc. IEEE Conf. Computer Vision and Pattern Recognition,* pages 144–152, Ann Arbor, Michigan, June 1988.

[8] S. Geman and D. Geman. Stochastic Relaxation, Gibbs Distributions, and the Bayesian Restoration of Images. IEEE *Trans. Pattern Analysis and Machine Intelligence,* 6(6):721–741, November 1984.

[9] W. E. L. Grimson. *From Images to Surface: A Computational Study of the Human Early Vision System.* MIT Press, Cambridge, Massachusetts, 1981.

[10] D. Keren and M. Werman. Variations on Regularization. In *Proc. 10th Intl. Conf. Pattern Recognition,* June 1990.

[11] I. Kweon, R. Hoffman, and E. Krotkov. Experimental Characterization of the Perceptron Laser Rangefinder. Technical Report CMU-RI-TR-91-1, Robotics Institute, Carnegie Mellon University, Pittsburgh, Pennsylvania, January 1991.

[12] B. Mandelbrot. *Fractals, Form, Chance, and Dimension.* Freeman, San Francisco, California, 1977.

[13] B. Mandelbrot. *The Fractal Geometry of Nature.* Freeman, San Francisco, California, 1982.

[14] J. L. Marroquin. Surface reconstruction preserving discontinuities. A. I. Memo 792, Massachusetts Institute of Technology, August 1984.

[15] A. Pentland. Fractal-Based Description of Natural Scenes. *IEEE Trans. on Pattern Analysis and Machine Intelligence*, 6(6):661–674, 1984.

[16] T. Poggio, V. Torre, and C. Koch. Computational vision and regularization theory. *Nature*, 317(6035):314–319, 26 September 1985.

[17] D. Saupe. Algorithms for Random Fractals. In H.-O. Peitgen and D. Saupe, editors, *The Science of Fractal Images*. Springer-Verlag, 1988.

[18] R Stevenson and E. Delp. Viewpoint Invariant Recovery of Visual Surfaces from Sparse Data. *IEEE Trans. Pattern Analysis and Machine Intelligence*, 14(9):897–909, September 1992.

[19] R Szeliski. Regularization uses fractal prior. In *Proc. AAAI-87: Sixth National Conf. Artificial Intelligence*, 1987.

[20] R Szeliski. *Bayesian Modeling of Uncertainty in Low-Level Vision*. Kluwer, Norwell, Massachusetts, 1989.

[21] D. Terzopoulos. *Multiresolution Computation of Visible-Surface Representations*. PhD thesis, Massachusetts Institute of Technology, January 1984.

[22] D. Terzopoulos. Computing Visible-Surface Representations. Technical Report A.I. Memo No. 800, Artificial Intelligence Laboratory, Massachusetts Institute of Technology, Cambridge, Massachusetts, March 1985.

[23] D. Tempoulos. Regularization of inverse visual problems involving discontinuities. *IEEE Trans. Pattern Analysis and Machine Intelligence*, 8(4):413–424, July 1986.

[24] N. Yokoya, K. Yamamoto, and N. Funakubo. Fractal-Based Analysis and Interpolation of 3D Natural Surface Shapes and Their Application to Terrain Modeling. *Computer Vision, Graphics, and Image Processing*, 46:284–302, 1989.